





Article

Reactivity Assessment of Modified Ferro Silicate Slag by R³ Method

Pithchai Pandian Sivakumar^{1,2,3}, Stijn Matthys¹, Nele De Belie¹ and Elke Gruyaert^{2,*}

- ¹ Magnel-Vandepitte Laboratory for Structural Engineering and Building Materials, Ghent University, Technologiepark Zwijnaarde 60, BE-9052 Ghent, Belgium; pithchaipandian.sivakumar@ugent.be (P.P.S.); stijn.matthys@ugent.be (S.M.); nele.debelie@ugent.be (N.D.B.)
- ² KU Leuven, Department of Civil Engineering, Materials and Constructions, Ghent Technology Campus, Gebroeders De Smetstraat 1, BE-9000 Ghent, Belgium
- ³ SIM vzw, Technologiepark 48, BE-9052 Zwijnaarde, Belgium
- * Correspondence: elke.gruyaert@kuleuven.be

Featured Application: Novel cementitious binder.

Abstract: Traditional methods to track the reactivity of supplementary cementitious materials (SCMs) and their contribution to the hydration mechanism mostly use Portland Cement (PC) as an activator. Alternatively, a novel method to assess the reactivity of SCMs called R³ was recently presented. This novel method uses lab grade chemicals such as portlandite (CH), K₂SO₄, KOH, and CaCO₃ to activate the SCM by resembling the pH of the alkaline pore solution created by PC. By using this method, the reactivity of the SCM can be easily quantified from measured heat release, bound water content, and CH consumption. The primary objective of the current study is to apply the novel methodology to analyze the reactivity of Modified Ferro Silicate (MFS) Cu slag benchmarked against siliceous fly ash (FA), ground granulated blast-furnace slag (GGBFS), and inert quartz filler. GGBFS showed the highest cumulative heat release and bound water content due to its latent hydraulic behavior. Determination with XRD analysis of the major phase of the R³ model MFS slag paste showed the participation of Fe in the hydration mechanism by forming Fe-AFm. R³ paste with GGBFS showed the presence of hydrotalcite/Al-AFm, whereas FA showed the presence of ettringite (AFt) as their crystalline reaction products. The experiments also indicate that the MFS slag acts as a reactive pozzolanic material with an acceptable performance in heat release, bound water content, and CH consumption, and can be used as SCM to make concrete. With the possibility of using MFS slag as SCM to replace part of PC, sustainability and circular economy can be fairly well achieved.

Keywords: modified ferro silicate slag; supplementary cementitious material; reactivity assessment; R³ method



Citation: Sivakumar, P.P.; Matthys, S.; De Belie, N.; Gruyaert, E. Reactivity Assessment of Modified Ferro Silicate Slag by R³ Method. *Appl. Sci.* **2021**, *11*, 366. <https://doi.org/10.3390/app11010366>

Received: 10 December 2020

Accepted: 29 December 2020

Published: 1 January 2021

Publisher's Note: MDPI stays neutral with regard to jurisdictional claims in published maps and institutional affiliations.



Copyright: © 2021 by the authors. Licensee MDPI, Basel, Switzerland. This article is an open access article distributed under the terms and conditions of the Creative Commons Attribution (CC BY) license (<https://creativecommons.org/licenses/by/4.0/>).

1. Introduction

Copper (Cu) is one of the most vital metals used in a wide range of thermal applications and electrical wiring. Cu metal is usually synthesized by pyro-metallurgical refining of Cu ore such as chalcopyrite (CuFeS₂) or bornite (Cu₅FeS₄) [1,2]. Alternatively, due to the improved technological facilities and state of the art on smelter and refining processes, industries also focus on the use of metal scraps as recyclable materials to synthesize Cu metal. During the smelting and refining of Cu ore or Cu rich metal scraps into Cu metal, a slag is obtained as a by-product [2]. This by-product is produced in high volume, as the production of 1 ton of Cu metal usually generates approximately 2.2–3.0 tons of Cu slag. Usually the slag is dumped, stockpiled, or to a limited extent used in low grade applications. Despite its limited usage, Cu slag (the term Cu slag in the literature refers to its origin, rather than its mineralogy, which is mainly a siliceous amorphous phase) is

widely used in abrasive tools, roofing granules, cutting tools, glass, and in the cement and concrete industry [3].

Global annual production of Portland Cement (PC), which contributes to 6–8% of the global CO₂ emissions, has reached over 4.5 billion tons, and is expected to increase to approximately 6 billion tons by end of 2030 [4–6]. This, together with the need for intensive energy in terms of electricity, explains the major environmental concerns and economic considerations related to the production of PC [7]. One of the possible solutions to decrease the environmental impact of the clinker production and to achieve a circular economy is the use of industrial by-products as a raw material source for replacement of cement.

Many researchers have investigated the use of industrial by-products as SCM [8–11]. Typical by-products used are materials possessing high content of amorphous phase (generally >90 wt%). Depending on the elemental composition of the amorphous phase, these by-products can be categorized as latent hydraulic (e.g., ground granulated blast-furnace slag (GGBFS)) or pozzolanic (e.g., fly ash (FA)) [12]. These compounds, if used in the concrete, can increase strength, improve durability behavior such as chloride ingress, and make concrete much ‘greener’ [13]. The term pozzolanic usually implies natural or artificial siliceous/aluminous material which reacts with H₂O in presence of Ca(OH)₂ [12]. Since a wide range of Cu slags are siliceous rich and have an amorphous structure, they can also be termed as pozzolanic. However, when Cu slags are added as SCM with PC, their mechanism and interaction with the cement phase is still not well understood.

Nevertheless, several publications have described the use of Cu slag as an alternative SCM and its influence on compressive strength [14,15]. In the work of Mobasher et al. [16], reactivity of the Cu slag was investigated by using PC and hydrated lime as activator. The final findings of Mobasher stated that the use of Cu slag delayed the initial strength development of the mortar made with a 15% replacement level of PC (at 1 and 7 days) while increasing the strength after 28 and 90 days. Arino et al. [17] examined the mechanical properties of concrete synthesized with Cu slag and PC. Concrete containing up to 15 wt% Cu slag as PC replacement with water to solid ratio of 0.4 was subjected to a compressive test. Compressive strength results showed a significant increase in the strength of the Cu slag incorporated concrete in comparison to the reference PC concrete after 160 days. Literature reveals that the usage of Cu slag as a SCM with PC increases the compressive strength at late ages (after 28 days). The contribution towards strength may generally be due to two reasons, those being: The pozzolanic behavior or the filler effect, although filler effect would be more pronounced at earlier ages. The filler effect is usually attributed to the fact that the surface of the SCMs grains acts as a nucleation site for the precipitation and growth of binder hydrates, which contribute to the increase in compressive strength [18,19].

There has been a wide range of traditional experimental techniques carried out to understand the reaction mechanism of SCMs, such as isothermal calorimetry, Chapelle test, Frattini test, and Strength Activity Index (SAI) [20–25]. For instance, Tironi et al. [22] studied the pozzolanic activity of calcined clay by direct pozzolanic methods such as Frattini and saturated lime test, and indirect methods such as SAI and electrical conductivity. As an important finding, the authors suggested that the Frattini test was found to be the most reliable method to assess the pozzolanic reactivity due to the fact that the Frattini test evaluates the CH consumption (related to pozzolanic reaction). In the work of Donatello et al. [23], pozzolanic activity of metakaolin, silica fume, fly ash, and incinerated sludge have been studied using the Frattini test, the saturated lime test and the strength activity index. In this scenario, the authors stated that no significant correlation could be found between the SAI test and saturated lime test results. In the recent work of Bouasria et al. [26], replacement of cement by Ferronickel slags (FNS) was investigated. It was observed that increasing the FNS content in the mix tends to decrease the compressive and flexural strength. Interestingly, the presence of higher silica content in the FNS leads to the formation of a higher polymerization degree of the silica chains in the C-S-H structures. In the recent work of Feng et al. [27], pozzolanic activity of granulated copper slag modified with CaO (GCS) was studied. The following were the interesting findings: (1) Paste

synthesized with PC-GCS showed increased heat release after seven days and compressive strength at 28 and 91 days, and (2) TGA and SEM analyses showed more gel phases and less pores in PC-GCS paste. In the work of Hallet et al. [28], the impact of slag fineness on the reactivity of blended cements with non-ferrous slag by R^3 was examined. It was stated that R^3 isothermal calorimetry showed that the slag was similar in reactivity to siliceous fly ash and increasing the fineness increases the reactivity of the slag.

Moreover, Pontes et al. [24] studied the pozzolanic reactivity of artificial pozzolanic materials by the Frattini method, Chapelle method, and SAI test. The reactivity was assessed for eight different materials of siliceous and aluminosilicates composition, and the authors stated that further investigation is needed to study the reaction mechanism of SCM due to the influence of clinker phases during the reactivity assessment. In the work of Edwin et al. [25], isothermal calorimetry, Chapelle test, Frattini test, and SAI test were used to assess the pozzolanic reactivity of Cu slag. The authors concluded that the pozzolanic activity of the Cu slag mainly depends on temperature, the curing age, and the specific surface area. In another recent work of Edwin et al. [29], porosity of reactive powder concrete (made with PC, copper slag, and additives) based on automated analysis of back-scattered-electron images was analyzed. However, the proposed analysis did not show similar results to the MIP data due to the different sizes and characteristics of the pores examined with MIP and back scattered electron images. The studies [21–25] used PC as an activator to study the reactivity of the SCM. Due to the influence of clinker phases on the reactivity assessment, only speculative conclusions can be made on the reactivity of the SCM. To overcome this drawback, a recent report [30] published by RILEM technical committee TC 267-TRM (which partly turned into the ASTM standard C1897-20 (2020)) proposed a novel method to evaluate the reactivity of SCMs. The method is termed as “ R^3 ”, which stands for rapid, reproducible, and relevant. The method uses mixes of SCM, CH, and H_2O , supplemented with alkali sulfate (SO_4^{2-}) and carbonate (CO_3^{2-}) resembling the pH of the alkaline pore solution created by PC. By using this method, the reactivity of the SCM can be easily quantified from measured heat release, bound water, and CH consumption. In this article, reactivity of Modified Ferro Silicate (MFS) Cu slag was assessed according to the novel R^3 model system reported in RILEM TC 267-TRM. Reactivity of the R^3 model MFS slag paste was compared with quartz filler and the widely used pozzolanic material siliceous FA and latent hydraulic SCM GGBFS. The R^3 model system was selected to eliminate the influence of PC while assessing the reactivity of the SCMs. The objective was to compare the reactive behavior of MFS slag with FA and GGBFS on the one hand and with inert filler on the other hand to understand its reaction mechanism, which should substantiate the use of MFS slag as a sustainable binder material for concrete.

2. Materials and Methods

2.1. Materials and Characterisation

Patented MFS slag was used as the starting material. MFS slag is a fumed secondary Cu slag synthesized during the recycling of Cu scraps into Cu metal. Initially, the MFS slag was dried in a laboratory oven at 105 °C for 24 h. Next, the dried MFS slag was milled in a attritor mill (Wiener 1S) to achieve a similar particle size distribution as PC. Quartz flour with a particle size distribution equivalent to MFS slag was also used as a starting material to synthesize the reference R^3 model sample. The particle size distribution was determined using a laser diffraction analyzer (Mastersizer 2000, Malvern Instrument Ltd.). Portland cement supplied by Holcim (CEM 52.5 N) and fly ash (class C) were used in this study. GGBFS, a by-product from the manufacture of iron, was supplied by Ecocem Benelux. Lab grade KOH, K_2SO_4 , and $CaCO_3$, along with $Ca(OH)_2$ (CH), which possesses less than 5 wt.% of $CaCO_3$, were used as the starting material to prepare the R^3 model paste. Initially, the chemical composition of the materials was determined by wavelength-dispersive X-ray fluorescence spectrometry (XRF). Mineralogical composition of all starting materials was obtained using X-ray diffraction (XRD, Thermo Scientific, ARL X'TRA). Quantitative XRD

analysis was carried out by using 10 wt.% of analytical grade crystalline ZnO (95% purity) as external standard. The material was blended with ZnO manually with the help of a mortar and pestle. An X-ray diffraction scan was recorded on the homogenized material using Cu K α radiation with acceleration voltage 30 kV, a current of 30 mA, a step size of 0.020°, and a counting time of 2.5 s per step. The diffraction pattern obtained using the XRD device was analyzed and quantified with Topas Academic V.5 software, using the Rietveld technique.

2.2. Synthesis of R³ Model Paste

The mix design used to synthesize R³ model paste as recommended by TC 267-TRM [1] is given in Table 1. Initially, the SCM was weighed and mixed with the CH and CaCO₃ gently using the spatula until a homogeneous color was achieved. KOH and K₂SO₄ were weighed and dissolved in the deionized H₂O. The prepared mix and solution were stored in an oven at 40 ± 2 °C for 24 h. After 24 h, the solution (pH around 13.6) was added to the dry powder and mixed at 1600 rpm for 2 min to achieve a homogeneous paste. The prepared paste was cast into an appropriate container, tapped gently to remove air bubbles. The container was covered with Parafilm M (plastic paraffin) to achieve a sealed layer and stored at 40 ± 2 °C for a period of 7 days to accelerate the reaction.

Table 1. Mix design for R³ model paste. SCM: Supplementary cementitious materials.

Component	SCM	CH	Deionized H ₂ O	KOH	K ₂ SO ₄	CaCO ₃
Mass (g)	11.11	33.33	60	0.24	1.2	5.56

2.3. Reactivity Assessment of the Synthesized R³ Model Paste

A primary objective to assess the reactivity by the R³ test was to avoid the influence of cement hydration on the SCMs and to assess the degree of reaction of SCMs individually. Here, the reactivity of the synthesized R³ paste was assessed by measuring: (1) Consumption of CH by ThermoGravimetric Analysis (TGA), (2) bound water by the oven method, (3) heat production rate by isothermal calorimetry, (4) pore solution analysis, and (5) presence of binder phase by XRD analysis.

2.3.1. CH Consumption Analysis for R³ Model Paste

Approximately 3 g of R³ hydrated model paste, cured for 7 days, was used to prepare the sample for TGA. The initial sample was crushed (1–3 mm) by mortar and pestle. The crushed sample was placed in 50 mL of isopropanol for 15 min for hydration stoppage through solvent exchange. The suspension (sample + isopropanol) was stirred constantly for a period of 2 min and vacuum filtration was carried out by a 2.7 µm pore size filter to separate the crushed sample from the isopropanol. The sample was placed on a watch glass and dried at 40 °C for 8 min in an oven. Next, the sample was stored in a low vacuum desiccator till the measurement was carried out. Approximately 50 mg of the stored sample was used for the TGA measurement. TGA was carried out in an Al₂O₃ crucible, with a heating regime of 30 to 950 °C at 10 °C/min in a N₂ atmosphere. Proteus thermal analysis software was used to measure the CH content vs. sample mass at 950 °C (m_{950}), using the tangential approach, with the mass loss attributed to CH ($\Delta m_{H_2O,CH}$) situated between 400 and 480 °C [31]. Three repetitions for a single measurement were carried out to calculate the mean value and standard deviation, and to check the reproducibility. Finally, residual CH ($m_{CH, ignited}$) and CH consumption ($m_{CH, consumption}$) (g/100 g SCM) of the SCM paste synthesized as per R³ model system are calculated by the Equations (1) and (2), respectively.

$$m_{CH, ignited} = 100 \times \frac{\Delta m_{H_2O,CH} \times 74.09}{18.02 \times m_{950}} \quad (1)$$

$$m_{CH,consumption} = 100 \times \frac{(m_{0,CH,ignited} - m_{CH,ignited})}{m_{0,SCM,ignited}} \quad (2)$$

2.3.2. Bound Water (Oven Method) for R³ Model Paste

A sample prepared and cured for 7 days as per the R³ procedure was used to measure the bound water content through heating using a laboratory oven. A sample, crushed (1–3 mm) by hand, was placed in an oven at 105 °C for 24 h and was used as a starting material. Prior to the experiment, the precise weight of the Al₂O₃ crucible, thermally treated at 350 °C for 1 h, termed as w_c , and the precise weight of the crucible with starting materials, termed as w_o , were determined.

The sample, along with the crucible, was calcined at 350 °C for 2 h in the box furnace. After 2 h, the oven was turned off and the sample was cooled till 150 °C. Final weight of the sample including the crucible was measured and termed as w_t . Finally the $H_2O_{bound, dried}$ was calculated (Equation (3)) and rescaled to g/100 g anhydrous ($H_2O_{bound, anhydrous}$) (Equation (4)).

$$H_2O_{bound, dried} = \frac{w_o - w_t}{w_o - w_c} \times 100 \quad (3)$$

$$H_2O_{bound, anhydrous} = \frac{H_2O_{bound, dried}}{(1 - H_2O_{bound, dried})} \quad (4)$$

2.3.3. Isothermal Calorimetry Protocol for R³ Model

The isothermal calorimetry technique (TAM Air, TA instruments) was used to investigate the reaction kinetics and to measure the heat production rate for the R³ model paste until the age of 7 days. The calorimeter was set to 40 °C and calibration was carried out after temperature was stabilized. All necessary equipment along with the materials used for the preparation of the samples was also placed in the oven at 40 °C. Exactly 9.405 g of deionized water was poured in the reference ampoule. After calibration, a sealed reference container was inserted in the reference channel of the calorimetric device. The baseline of the calorimetry was measured for 3 h. Fifteen g (termed as m_p) of R³ model paste was introduced into the ampoule, immediately after mixing, and inserted in the measuring channel of the calorimeter. The heat profile was recorded at 40 °C for 7 days. The cumulative heat of the sample was calculated by neglecting the initial 1.2 h due to the mixing at 20 °C, which causes initial negative flow. The cumulative heat release is obtained in J/g SCM as given by Equation (5).

$$cumulative\ heat\ release = \frac{Heat\ released}{(m_p \times 0.0997)} \quad (5)$$

0.0997 in the denominator corresponds to the ratio of SCM present in the R³ model paste.

2.3.4. XRD and Pore Solution Analysis

X-ray diffraction scans with a step size 0.020° and counting time of 2.5 s per step in a 2θ range from 5° to 15° were recorded on the 7 days old hydration stopped R³ samples to investigate the presence of crystalline binder phases. Pore fluid from the hydration stopped MFS slag—R³ samples was also extracted with a pressure up to 200 MPa. After extraction, the pore solution was filtered and diluted with acid. The diluted solutions were analyzed using ICP-OES.

2.3.5. Synthesis of Mortar

Compressive strength was assessed on PC, 15 M, 30 M, 50 M, and 70 M mortars, prepared as per EN 196-1 and cured at 20 ± 1 °C and 95% relative humidity for 24 h (Table 2). For the mortar with 70 wt.-% MFS slag in the binder, additional powder activation by Na₂SO₄ was foreseen, resulting in a hybrid mortar (HM). After 24 h, the mortars were

demolded and stored in a curing chamber at 20 ± 1 °C and 95% relative humidity until the compressive strength tests were performed.

Table 2. Binder composition in wt.%. PC: Portland cement; MFS: Modified Ferro Silicate.

Mortar	PC	MFS	Na ₂ SO ₄
PC	100	0	0
15 M	85	15	0
30 M	70	30	0
50 M	50	50	0
70 M	69	29	2

3. Results and Discussion

3.1. Characterization of the Starting Materials

Chemically, the starting materials are mainly composed of four oxides of Si, Fe, Al, and Ca (Table 3). MFS, GGBFS, and FA are SiO₂ rich by-products with varying oxide contents of Fe, Al, and Ca. However, MFS slag still possesses a high amount of Fe₂O₃ and around 2–4 wt.% of ZnO and GGBFS contains nearly 41 wt.% of CaO. Quartz flour is the inert filler containing only oxides of Si. Amorphous and crystalline content of the starting materials are shown in Table 4. Since MFS and GGBFS are industrial by-products obtained by a quenching process, they are mainly composed of an amorphous or glassy phase. FA is an amorphous rich by-product synthesized during the coal combustion that is mainly composed of fine particulates which are collected by the electrostatic precipitator. In this study, siliceous rich FA of Class F was used to see the relative comparison with MFS slag. Particle size distribution of the starting materials is shown in Table 5.

Table 3. Chemical composition of the starting materials in wt.%. GGBFS: Ground granulated blast-furnace slag; FA: Fly ash.

Component	MFS	GGBFS	FA	Quartz
SiO ₂	32.3	35.7	54.3	99.2
Fe ₂ O ₃	40.9	0.9	10.2	-
Al ₂ O ₃	11.0	11.9	22.7	-
CaO	3.9	41.3	4.2	-
Others	11.9	10.2	8.6	0.8

Table 4. Amorphous and crystalline content of the starting materials in wt.%.

Phase	MFS	GGBFS	FA	Quartz
Amorphous	92	96.5	75	3
Crystalline	8	3.5	25	97

Table 5. Particle size distribution of the starting materials.

Starting Materials	Particle Size Distribution		
	d ₁₀ (µm)	d ₅₀ (µm)	d ₁₀₀ (µm)
MFS	2.9	12	45.5
GGBFS	2.8	17.2	42.5
FA	2.3	18.6	81.2
Quartz	3.7	10.9	40.2

3.2. Reactivity Assessment of R³ Model Paste

3.2.1. CH Consumption and Bound Water

The calculated CH content is shown in Table 6. From this, it can be seen that all SCMs and inert quartz filler consumed CH at a different degree compared to its initial presence.

R³ paste synthesized from MFS slag has consumed less CH than the well-established pozzolanic source FA. MFS slag has an amorphous phase that is rich in SiO₂ (around 30 wt%). However, although fly ash has lower amorphous content than MFS slag, it contains more SiO₂ (around 50 wt%, assuming all SiO₂ is present in glass phase). Initially, Ca(OH)₂ is dissolved in presence of H₂O to release Ca²⁺ ions which consume the Si²⁺ ions (or silicates with different degrees of H dissociation) from MFS slag to produce C-S-H as a result of the pozzolanic mechanism. Furthermore, due to the presence of a minor content of Al₂O₃ in the MFS slag, C-S-H can take-up aluminate ions to form C-A-S-H.

Table 6. Reactivity assessment of R³ model paste—CH consumption calculated from ThermoGravimetric Analysis (TGA) analysis and Bound water calculated by oven method.

R ³ Model Paste	CH Consumption (g/100 g SCM)		Bound Water (g/100 g SCM)	
	Mean	Std.dev.	Mean	Std.dev.
MFS	55	8	5.3	1.2
FA	72	7	3.5	0.8
GGBFS	48	6	7.4	1.9
Quartz	5	2	0.3	0.2

GGBFS shows less CH consumption compared to the MFS slag and FA due to the latent hydraulic behavior. Due to the presence of a reactive amorphous phase rich in CaO and SiO₂, GGBFS has the potential to self react with H₂O to produce C-S-H or C-A-S-H binder phase [32]. Bound water calculated by the oven method also shows that GGBFS paste possessed a high amount of hydrated compounds, which decomposed between 105 and 350 °C, compared to MFS slag and FA (Table 6). However, by considering this temperature range, certain hydrates such as ettringite cannot be taken into account. Ettringite dehydrates below 100 °C as mentioned elsewhere [33,34]. Note that the mechanism governing GGBFS reactivity explained through CH consumption and bound water cannot be considered as decisive, and the results should be interpreted with caution by accounting the results shown in Sections 3.2.2 and 3.2.3. A slight decrease in the CH content compared to the initial presence was observed with the quartz filler material. This indicates that the amorphous phase (around 3 wt.%) of quartz can consume a small amount of CH to produce C-S-H, and this mechanism might be due to the high temperature curing (40 °C). For instance, different authors have described the mechanism of decrease in the CH content with increased ages of the inert filler (quartz) blended system [35–37]. Additionally, the study published by Li et al. [30] to assess the reactivity using the R³ model system showed slight CH consumption for quartz inert filler.

3.2.2. Isothermal Calorimetry

Figure 1 shows the calorimetric data of the R³ model paste containing MFS slag, GGBFS, FA, and quartz filler expressed per g of SCM. GGBFS shows a higher heat production rate than MFS, FA, and quartz. The following observations can be made on their reactivity:

- (1) GGBFS paste is prone to dissolve by itself in H₂O and can synthesize more binder such as C-S-H or C-A-S-H, AFm, and AFt, which results in a strong exothermic heat release. Bound water analysis of GGBFS explained in Section 3.2.1 also showed that GGBFS possessed a high amount of hydrates.
- (2) MFS slag paste shows increased heat release in comparison to FA. This behavior is attributed to the presence of a higher content of reactive amorphous phase (as shown in Table 4), possibly suggesting faster dissolution of the reactive phase and formation of binder.
- (3) As the MFS slag has released substantially more heat compared to inert filler, this indicates that extra heat release is probably due to the pozzolanic reaction (Figure 1b).

- (4) The inert quartz filler proved to be a comprehensive inert material to investigate the filler effect due to its limited heat production attributed to its CH consumption observed in Figure 1a).

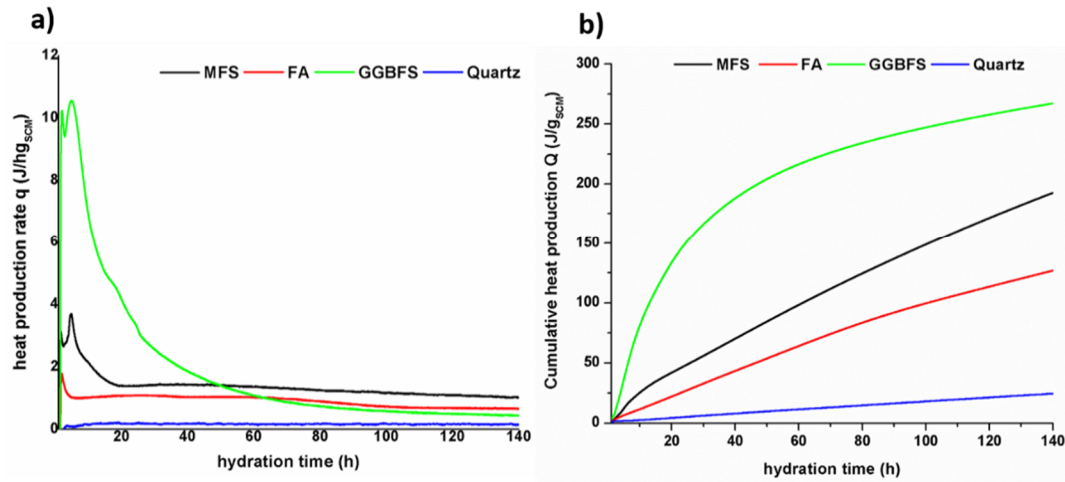


Figure 1. Calorimetric analysis of the R³ model paste: (a) Heat production rate in J/(h·g_{scm}) vs. hydration time (h); (b) cumulative heat production in J/(g_{scm}) vs. hydration time (h).

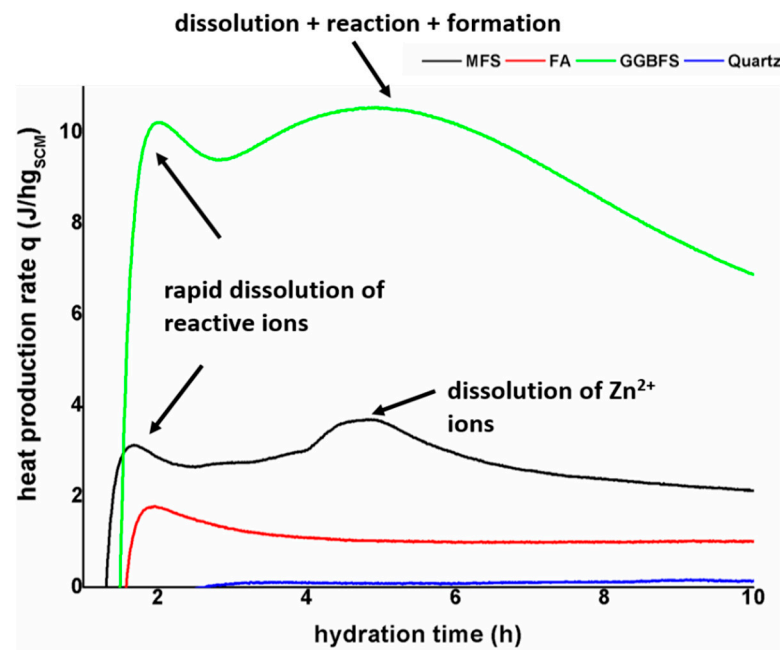


Figure 2. Calorimetric analysis of the R³ model paste for initial 10 h.

From Figure 2, the heat production rate of the R³ model paste can be categorized into two regions: (1) Initial heat release up to 2 h, likely due to the dissolution of reactive ions such as SO_4^{2-} , Al^{3+} , and CO_3^{2-} , (2) later heat release until 10 h, likely attributed to the gradual dissolution of the amorphous phase and the formation of binder phases such as C-S-H or C-A-S-H, AFt, and AFm. This heat release intensity tends to differ for FA due to the increased presence of crystalline phases (25 wt.%) which act as a barrier for the dissolution of the amorphous phase. For instance, Chancey et al. [38] characterized the amorphous and crystalline phases of the FA class F and showed that the amorphous phase was partially surrounded by crystalline phases such as quartz, mullite, and maghemite, thus limiting the dissolution and reaction towards formation of binder. Heat release till 10 h is only seen with MFS slag, GGBFS, FA, and not with inert filler, suggesting that this relates

to the dissolution of amorphous (glassy) phases to form hydrates. Moreover, R³ model paste incorporating MFS slag showed an increased heat release in the period between 4 to 6 h. This heat release can possibly be attributed to the dissolution of Zn²⁺ ions present in the MFS slag. For instance, ZnO present in the glassy structure of the MFS slag could potentially tend to dissolve and influence the hydration mechanism.

3.2.3. Influence of Zn²⁺ in the Hydration Mechanism of MFS Slag

Several authors have reported the influence of Zn²⁺ in PC and alkali activated materials [39–44]. For instance, Gawlicki et al. [44] studied the hydration of PC in the presence of ZnO and found that amorphous Zn(OH)₂ could be formed in the reaction with H₂O, which could potentially transform into Ca(Zn(OH)₃)₂·2H₂O, provoking the heat release. In addition, Trezza et al. [42] studied the hydration products of the PC in presence of Zn²⁺ ions with infrared (IR) spectroscopy showing the existence of Ca(Zn(OH)₃)₂·2H₂O species. The authors also concluded that Zn in presence of H₂O can react to form Zn(OH)₂ which has additional hydroxyl ions producing a complex oxyanion which may precipitate as an insoluble Ca(Zn(OH)₃)₂·2H₂O salt. Moreover, a recent study [43] showed the mechanism of ZnO in GGBFS based alkali activated materials through X-ray pair distribution function. The proposed mechanism by the authors states that ZnO dissolves in the highly alkaline solution, reacting with the dissolved Ca²⁺ ions from the slag to form Ca(Zn(OH)₃)₂·2H₂O. This mechanism continues as long as there is availability of free Zn in the pore solution. This proposed mechanism can be applicable to the MFS slag due to the presence of Zn²⁺ ions in the glassy phase. Upon addition of H₂O in the R³ mix containing MFS slag as SCM, Zn²⁺ (from MFS slag) and Ca²⁺ (from Ca(OH)₂, CaCO₃, MFS) slowly tend to dissolve into the solution and eventually form Ca(Zn(OH)₃)₂·2H₂O, which results in an exothermic reaction and heat release. This mechanism is expected to continue until all free ZnO present in the glass is consumed.

3.2.4. Pore Solution vs. Calorimetric Analysis

The diluted pore solution from the R³ model MFS slag paste has been extracted at a curing age of 7 days and analyzed to determine the concentration of Si and Zn (Table 7). The ICP-OES analysis showed the presence of Zn that is possibly dissolved from the MFS slags. The Si concentration in the pore solution also implies the pozzolanic reactivity of the slag. Moreover, in another study [45], we have analyzed the reactivity of MFS slag along with thermally and chemically adapted MFS slag through R³ calorimetric analysis. In this work, a distinct increased heat release between 4 to 6 h in the calorimetric analysis is only observed for the reference MFS slag; the thermally adapted MFS slag, which has less ZnO, showed no increased heat release in the specified time window. This supports the conclusion that this part of the heat release in the MFS slag is related to the presence of Zn²⁺ ions in the glassy phase.

Table 7. Elemental concentrations of aqueous pore solution for MFS slag R³ paste.

Element	Concentration of Elements (mmol/L)
Zn	7
Si	53

3.2.5. XRD Analysis

The XRD analysis in Figure 3 shows the presence of hydrated phases in the R³ paste after 7 days curing. The main hydration products of the R³ hydrated paste may include C-(A)-S-H, AFt, and AFm phases depending on the chemical composition of the starting SCM. General expected AFm phases are hydroxy-AFm, Al-hemicarbonate (Al-Hc), and Al-monocarbonate (Al-Mc). It has been reported elsewhere [46,47] that Al-Hc and hydroxy-AFm are unstable with respect to Al-Mc in the presence of CaCO₃, and [48]

showed that with rising CO_3^{2-} ion concentration, hemicarbonates (Hc) are transformed into monocarbonates (Mc).

In the FA containing model R^3 system, a sharp and distinct peak of ettringite ($2\theta = 9.1^\circ$) was observed. Ettringite can be synthesised in a system by reacting stoichiometric amounts of Ca^{2+} , SO_4^{2-} , and Al^{3+} ions with H_2O [49,50] and formation of ettringite in FA is mainly attributed to the high content of Al_2O_3 . However, no presence of AFm phase can be observed in FA due to the fact that FA just reacts so slowly that the SO_4^{2-} ions were not completely consumed, thus maintaining the saturation index which can stabilise the AFt (ettringite) phase [51]. In the GGBFS system, monocarboaluminate (Al-Mc) along with hydrotalcite (HT) can be observed, where the added calcite is the carbonate source to form these AFm phases. Some literature has observed the transformation of hemicarbonates (Hc) to monocarbonates (Mc) happening in the period between 14 to 28 days [46,52]. However, R^3 model paste of GGBFS showed the presence of monocarboaluminate even after 7 days due to the presence of excess CO_3^{2-} ions with an accelerating curing condition at $40 \pm 2^\circ\text{C}$. Due to the presence of MgO in GGBFS, Mg^{2+} ions in the presence of Al^{3+} and CO_3^{2-} most likely form hydrotalcite (HT). Due to the poor crystalline nature of C-S-H and the possible incorporation of other ions such as Al^{3+} when the C-S-H formed, presence of this amorphous C-S-H cannot be validated by XRD analysis. Finally, all crystalline hydrated binder phases discussed are not seen in the quartz based R^3 paste, indicating its inert behavior.

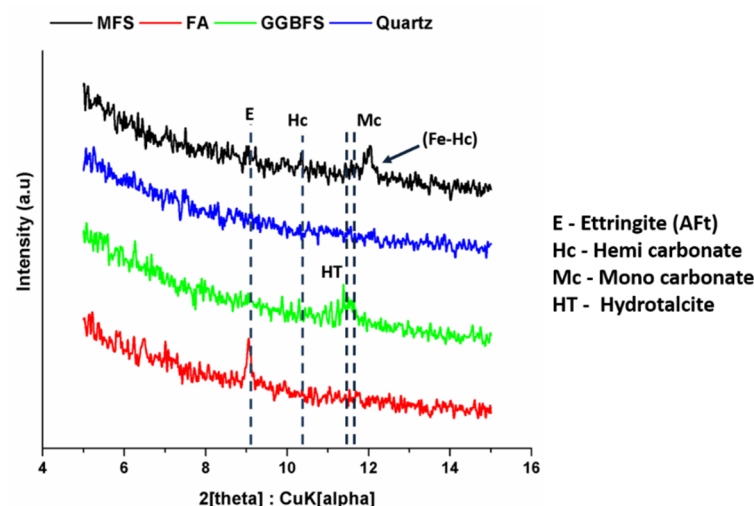


Figure 3. XRD analysis R^3 model paste after 7 days.

MFS slag contains around 40 to 41 wt% Fe_2O_3 . During hydration, Fe containing AFm and/or Fe-AFt phases may form [53]. As seen in the XRD analysis around $2\theta = 10.3^\circ$, it is known from literature that Al containing AFm phases (generally Al-Hc) are formed first and later converted to Al-Mc ($2\theta = 11.8^\circ$) with an increase in CO_3^{2-} content as seen in GGBFS [47]. However, this peak of $2\theta = 11.8^\circ$ has undergone a shift in the MFS slag and it is seen at $2\theta = 12.2^\circ$, possibly indicating that the observed phase could correspond to Fe-Hc and not Al-Mc. However, further experimental research such as Mössbauer and Raman spectroscopy are needed to verify the formation of Fe-Hc.

The R^3 mix design releases ions such as Ca^{2+} , SO_4^{2-} , CO_3^{2-} upon contact with H_2O . The released ions dissolve the SCM to form corresponding hydrated binder phases depending on its chemical composition. For instance, SCM possessing $\text{FeO}/\text{Fe}_2\text{O}_3$ and SiO_2 initially dissolves to release $\text{Fe}^{2+}/\text{Fe}^{3+}$ and Si^{2+} ions, which later react with Ca^{2+} , SO_4^{2-} , CO_3^{2-} , OH^- to form C-S-H and Fe-Mc and/or Hc. If the SCM mainly consists of Al_2O_3 and SiO_2 such as, for instance, FA, Al^{3+} ions react with Ca^{2+} , SO_4^{2-} to form ettringite (AFt), and then the C-S-H can take up remaining Al^{3+} ions to form C-(A)-S-H. Chemistry of the GGBFS includes oxides of Al, Ca, and Si along with Mg. For instance, Mg^{2+} in the presence of Al^{3+} and CO_3^{2-} ions tends to form hydrotalcite-like phases, and

Al^{3+} in presence of CO_3^{2-} and Ca^{2+} forms Al-Mc and/or Hc. However, the role of $CaCO_3$ in the hydration mechanism is still an open discussion. Different authors have already published their hypotheses, but there is no general agreement on the role of $CaCO_3$ during cement hydration [54–56]. An interesting study [57] proposed two possible hypotheses by modelling and calculating the role of $CaCO_3$ in cement hydration. They proposed that the role of $CaCO_3$ has two functions: (1) Active participant, and (2) inert participant. With respect to their findings, XRD results of the presented work can be interpreted as follows. As an active participant, the $CaCO_3$ present in the R^3 mix tends to dissolve and releases CO_3^{2-} into pore solution forming AFm phases, as is the case for GGBFS and MFS slag. As an inert participant, the $CaCO_3$ tends to just act as an inert filler or reacts slowly after 7 days without participating in the short term reaction mechanisms as in the case for FA.

4. Implementation of MFS Slag as Sustainable Binder in Mortar and Concrete—Strength and Ecological Benefits

Mortar with replacement levels of 15, 30, and 50 wt% of PC by MFS-slag were prepared to evaluate the compressive strength in function of time (Table 8). SCM mortar synthesized from MFS slags showed a slow increase in compressive strength from 2 days to 7 days, and a high increase in the period from 7 to 91 days compared to the reference PC value. Especially from the age of 28 days, the MFS slag clearly contributes to the strength, since the mixes with 15%, 30%, and 50% MFS slag reach higher compressive strength than the nominal reference values corresponding to 85%, 70%, and 50% of the PC compressive strength. This foreseen strength development is due to the possible mechanism of slow dissolution of amorphous silica from MFS slag in the alkaline pore solution and the formation of strength providing phases such as C-S-H and C-A-S-H as mentioned in Sections 3.2.1 and 3.2.4. Moreover, mortar with MFS slag with a replacement level of 70 wt% of MFS slag in PC with presence of solid activators (Na_2SO_4) were prepared to study their compressive strength. Strength development of hybrid mortar (HM) also showed similar trends to the SCM mortars. However, HM mortars showed improved strength in comparison with 50 wt% MFS-slag SCM mortars after 28 days. This is due to the combined effect of pozzolanic and (geo)polymeric reaction. Nevertheless, HM mortars showed lower strength after 91 days with respect to 50 wt% MFS-slag SCM mortars.

Table 8. Compressive strength of MFS slag mortars in MPa (in function of wt% of MFS slag vs. total binder). HM: Hybrid mortar.

Days	PC Mortar		SCM Mortar		HM Mortar
	0%	15%	30%	50%	70%
2	38 ± 2.2	32 ± 1.7	30 ± 2.4	18 ± 0.8	20 ± 1.1
7	58 ± 1.9	42 ± 3.1	42 ± 2.7	30 ± 1.4	34 ± 2.5
28	69 ± 3.2	61 ± 2.5	58 ± 2.9	40 ± 1.7	45 ± 2.5
91	72 ± 1.2	67 ± 3.4	63 ± 1.5	53 ± 2.9	48 ± 1.5

With respect to the increase in the global annual production of PC, global CO_2 emissions are also expected to increase to approximately 6 billion tons by the end of 2030. These MFS slags, if used in the concrete, can make the material much ‘greener’. MFS slag can be incorporated in concrete as SCM or with additional activation, depending on the application. Partial replacement of PC up to certain replacement levels can be achieved without comprising the mechanical properties of the concrete (or at least with no larger effect than expected for traditional SCMs). However, a larger replacement level of around 70 wt% of MFS slag in PC can also be achieved with activation. At the same time, a by-product from Cu industry finds a high-level application. With less cement used to make concrete and the possibility of using MFS slag as SCM, sustainability and circular economy can be fairly well achieved.

5. Conclusions

The presented work gives a deep insight into the reactivity of a novel SCM, namely a fumed secondary copper slag called MFS slag. Reactivity of the MFS slag was successfully assessed by the recently developed R^3 model technique. The R^3 model paste designed by RILEM for assessing the reactivity of the SCMs allows us to overcome the limitations of the traditional reactivity test methods with PC-based pastes. From the R^3 model analysis, it was found that MFS slag can be regarded as a pozzolanic SCM due to its reactive behavior and can be used as SCM to make concrete.

The following can be stated as important findings from this work:

- (1) Bound water analysis of the R^3 model paste showed that GGBFS and MFS slag possess a high amount of binder hydrates due to their latent hydraulic and pozzolanic behavior, respectively. These hydrates decomposed between 105 and 350 °C during the thermal treatment.
- (2) CH consumption studied by TGA analysis showed that MFS slag had similar pozzolanic properties as other traditional SCMs.
- (3) R^3 calorimetric analysis indicated that MFS slag provoked a cumulative heat release in the range between FA and GGBFS (although some of the heat release could be due to the presence of Zn). Inert filler of quartz showed almost no heat release with R^3 calorimetric analysis, corresponding with consumption of only a slight amount of CH found by TGA analysis.
- (4) XRD analysis of the R^3 model MFS slag indicated the participation of “Fe” in the hydration mechanism and the existence of Fe-AFm, next to other hydrated binder phases.

One of the main research priorities in the future is to better understand the dissolution and role of ZnO and Fe₂O₃ in the hydration mechanism of MFS slags, and the role of CaCO₃ in the formation of AFt/AFm phases for the R^3 model paste. In this respect, future experimental research such as Mössbauer and Raman spectroscopy analysis are needed to verify the participation of Fe₂O₃ and ZnO in the hydration mechanism. Future research is also needed to verify the performance over long time scales, including complete durability assessment such as resistance to chloride and alkali silica reaction.

Author Contributions: Conceptualization: N.D.B., S.M., E.G., P.P.S.; methodology: P.P.S., N.D.B., S.M., E.G.; formal analysis and investigation: P.P.S.; writing—original draft preparation: P.P.S.; writing—review and editing: N.D.B., S.M., E.G.; funding acquisition: S.M., N.D.B., E.G.; resources: N.D.B., S.M.; supervision: S.M., N.D.B., E.G. All authors have read and agreed to the published version of the manuscript.

Funding: This research was funded by the SIM MARES program (DUSC project), grant number HBC.2017.0607.

Institutional Review Board Statement: Not applicable.

Informed Consent Statement: Not applicable.

Data Availability Statement: The data presented in this study are available on request from the corresponding author. The data are not publicly available due to the SIM ICON Project Agreement DUSC (HBC.2017.0607), Contract ref. A18TT1346.

Acknowledgments: The authors would like to acknowledge the industrial partner Resourcefull for providing raw materials. The authors would also like to thank SCRiPTS and COMOC research groups, Department of Chemistry, Ghent University for assisting with the TGA and XRD measurements.

Conflicts of Interest: The authors declare no conflict of interest.

References

1. Davenport, W.; King, M.; Schlesinger, M.; Biswas, A. *Chemical Metallurgy of Copper*; Elsevier: Amsterdam, The Netherlands, 2002; pp. 327–339. [[CrossRef](#)]
2. Schlesinger, M.E.; King, M.J.; Sole, K.C.; Davenport, W.G. *Extractive Metallurgy of Copper*; Elsevier: Amsterdam, The Netherlands, 2011. [[CrossRef](#)]

3. Gorai, B.; Jana, R. Premchand Characteristics and utilisation of copper slag—A review. *Resour. Conserv. Recycl.* **2003**, *39*, 299–313. [[CrossRef](#)]
4. Worrell, E.; Price, L.; Martin, N.; Hendriks, C.; Meida, L.O. Carbon dioxide emissions from the global cement industry. *Annu. Rev. Energy Environ.* **2001**, *26*, 303–329. [[CrossRef](#)]
5. US Geological Survey; Orienteering, S. *Mineral Commodity Summaries*; Government Printing Office: Washington, DC, USA, 2017. [[CrossRef](#)]
6. Benhelal, E.; Zahedi, G.; Shamsaei, E.; Bahadori, A. Global strategies and potentials to curb CO₂ emissions in cement industry. *J. Clean. Prod.* **2013**, *51*, 142–161. [[CrossRef](#)]
7. Schneider, M.; Romer, M.; Tschudin, M.; Bolio, H. Sustainable cement production—Present and future. *Cem. Concr. Res.* **2011**, *41*, 642–650. [[CrossRef](#)]
8. Lothenbach, B.; Scrivener, K.; Hooton, R. Supplementary cementitious materials. *Cem. Concr. Res.* **2011**, *41*, 1244–1256. [[CrossRef](#)]
9. Irassar, E.F.; González, M.; Rahhal, V.F. Sulphate resistance of type V cements with limestone filler and natural pozzolana. *Cem. Concr. Compos.* **2000**, *22*, 361–368. [[CrossRef](#)]
10. Ogirigbo, O.R.; Black, L. Influence of slag composition and temperature on the hydration and microstructure of slag blended cements. *Constr. Build. Mater.* **2016**, *126*, 496–507. [[CrossRef](#)]
11. Trauchesse, R.; Mechling, J.-M.; LeComte, A.; Roux, A.; Le Rolland, B. Hydration of ordinary Portland cement and calcium sulfoaluminate cement blends. *Cem. Concr. Compos.* **2015**, *56*, 106–114. [[CrossRef](#)]
12. Massazza, F. Pozzolana and Pozzolanic Cements. *Leas Chem. Cement Concrete* **1998**, 471–635. [[CrossRef](#)]
13. Papadakis, V.G. Effect of supplementary cementing materials on concrete resistance against carbonation and chloride ingress. *Cem. Concr. Res.* **2000**, *30*, 291–299. [[CrossRef](#)]
14. Taha, R.A.; Alnuaimi, A.S.; Al-Jabri, K.; Al-Harthy, A. Evaluation of controlled low strength materials containing industrial by-products. *Build. Environ.* **2007**, *42*, 3366–3372. [[CrossRef](#)]
15. Al-Jabri, K.; Taha, R.; Al-Hashmi, A.; Al-Harthy, A. Effect of copper slag and cement by-pass dust addition on mechanical properties of concrete. *Constr. Build. Mater.* **2006**, *20*, 322–331. [[CrossRef](#)]
16. Mobasher, M.B.; Devaguptapu, M.A.R. Effect of Copper Slag on the Hydration of Blended Cementitious Mixtures. In Proceedings of the 1996 4th Materials Engineering Conference. Part 2 (of 2), Washington, DC, USA, 10–14 November 1996.
17. Ariño, A.M.; Mobasher, B. Effect of ground copper slag on strength and toughness of cementitious mixes. *ACI Mater. J.* **1999**, *96*, 68–73.
18. Juenger, M.C.; Siddique, R. Recent advances in understanding the role of supplementary cementitious materials in concrete. *Cem. Concr. Res.* **2015**, *78*, 71–80. [[CrossRef](#)]
19. Scrivener, K.; Juilland, P.; Monteiro, P.J. Advances in understanding hydration of Portland cement. *Cem. Concr. Res.* **2015**, *78*, 38–56. [[CrossRef](#)]
20. Khayat, K.H.; Meyer, C.; Behnood, A. Utilization of copper slag in cement and concrete. *Resour. Conserv. Recycl.* **2008**, *52*, 1115–1120. [[CrossRef](#)]
21. Agarwal, S. Pozzolanic activity of various siliceous materials. *Cem. Concr. Res.* **2006**, *36*, 1735–1739. [[CrossRef](#)]
22. Tironi, A.; Trezza, M.A.; Scian, A.N.; Irassar, E.F. Assessment of pozzolanic activity of different calcined clays. *Cem. Concr. Compos.* **2013**, *37*, 319–327. [[CrossRef](#)]
23. Donatello, S.; Tyrer, M.; Cheeseman, C. Comparison of test methods to assess pozzolanic activity. *Cem. Concr. Compos.* **2010**, *32*, 121–127. [[CrossRef](#)]
24. Pontes, J.; Silva, A.S.; Faria, P. Evaluation of Pozzolanic Reactivity of Artificial Pozzolans. *Mater. Sci. Forum* **2012**, 433–438. [[CrossRef](#)]
25. Edwin, R.S.; De Schepper, M.; Gruyaert, E.; De Belie, N. Effect of secondary copper slag as cementitious material in ultra-high performance mortar. *Constr. Build. Mater.* **2016**, *119*, 31–44. [[CrossRef](#)]
26. Bouasria, M.; Khadraoui, F.; Benzaama, M.-H.; Touati, K.; Chateigner, D.; Gascoin, S.; Pralong, V.; Orberger, B.; Babouri, L.; El Mendili, Y. Partial substitution of cement by the association of Ferronickel slags and *Crepidula fornicata* shells. *J. Build. Eng.* **2021**, *33*, 101587. [[CrossRef](#)]
27. Feng, Y.; Yang, Q.; Chen, Q.; Kero, J.; Andersson, A.; Ahmed, H.; Engström, F.; Samuelsson, C. Characterization and evaluation of the pozzolanic activity of granulated copper slag modified with CaO. *J. Clean. Prod.* **2019**, *232*, 1112–1120. [[CrossRef](#)]
28. Hallet, V.; De Belie, N.; Pontikes, Y. The impact of slag fineness on the reactivity of blended cements with high-volume non-ferrous metallurgy slag. *Constr. Build. Mater.* **2020**, *257*, 119400. [[CrossRef](#)]
29. Edwin, R.S.; Mushthofa, M.; Gruyaert, E.; De Belie, N. Quantitative analysis on porosity of reactive powder concrete based on automated analysis of back-scattered-electron images. *Cem. Concr. Compos.* **2019**, *96*, 1–10. [[CrossRef](#)]
30. Li, X.; Snellings, R.; Antoni, M.; Alderete, N.M.; Haha, M.B.; Bishnoi, S.; Cizer, Ö.; Cyr, M.; De Weerd, K.; Dhandapani, Y.; et al. Reactivity tests for supplementary cementitious materials: RILEM TC 267-TRM phase 1. *Mater. Struct.* **2018**, *51*, 151. [[CrossRef](#)]
31. Scrivener, K.; Snellings, R.; Lothenbach, B. *A Practical Guide to Microstructural Analysis of Cementitious Materials*; CRC Press: Boca Raton, FL, USA, 2018.
32. Özbay, E.; Erdemir, M.; Durmuş, H.I. Utilization and efficiency of ground granulated blast furnace slag on concrete properties—A review. *Constr. Build. Mater.* **2016**, *105*, 423–434. [[CrossRef](#)]

33. Mantellato, S.; Palacios, M.; Flatt, R.J. Impact of sample preparation on the specific surface area of synthetic ettringite. *Cem. Concr. Res.* **2016**, *86*, 20–28. [[CrossRef](#)]
34. Théréne, F.; Keita, E.; Naël-Redolfi, J.; Boustingorry, P.; Bonafous, L.; Roussel, N. Water absorption of recycled aggregates: Measurements, influence of temperature and practical consequences. *Cem. Concr. Res.* **2020**, *137*, 106196. [[CrossRef](#)]
35. Cyr, M.; Lawrence, P.; Ringot, E. Mineral admixtures in mortars. *Cem. Concr. Res.* **2005**, *35*, 719–730. [[CrossRef](#)]
36. Deboucha, W.; Leklou, N.; Khelidj, A.; Oudjit, M.N. Hydration development of mineral additives blended cement using thermogravimetric analysis (TGA): Methodology of calculating the degree of hydration. *Constr. Build. Mater.* **2017**, *146*, 687–701. [[CrossRef](#)]
37. Zheng, K. Pozzolanic reaction of glass powder and its role in controlling alkali–silica reaction. *Cem. Concr. Compos.* **2016**, *67*, 30–38. [[CrossRef](#)]
38. Chancey, R.T.; Stutzman, P.; Juenger, M.C.; Fowler, D.W. Comprehensive phase characterization of crystalline and amorphous phases of a Class F fly ash. *Cem. Concr. Res.* **2010**, *40*, 146–156. [[CrossRef](#)]
39. Asavapisit, S.; Fowler, G.; Cheeseman, C. Solution chemistry during cement hydration in the presence of metal hydroxide wastes. *Cem. Concr. Res.* **1997**, *27*, 1249–1260. [[CrossRef](#)]
40. Hill, J.; Sharp, J. The hydration products of Portland cement in the presence of tin(II) chloride. *Cem. Concr. Res.* **2003**, *33*, 121–124. [[CrossRef](#)]
41. Stephan, D.; Maleki, H.; Knöfel, D.; Eber, B.; Härdtl, R. Influence of Cr, Ni, and Zn on the properties of pure clinker phases. *Cem. Concr. Res.* **1999**, *29*, 651–657. [[CrossRef](#)]
42. Trezza, M.A. Hydration study of ordinary portland cement in the presence of zinc ions. *Mater. Res.* **2007**, *10*, 331–334. [[CrossRef](#)]
43. Garg, N.; White, C.E. Mechanism of zinc oxide retardation in alkali-activated materials: An in situ X-ray pair distribution function investigation. *J. Mater. Chem. A* **2017**, *5*, 11794–11804. [[CrossRef](#)]
44. Gawlicki, M.; Czamarska, D. Effect of ZnO on the hydration of Portland cement. *J. Therm. Anal. Calorim.* **1992**, *38*, 2157–2161. [[CrossRef](#)]
45. Sivakumar, P.P.; Matthys, S.; De Belie, N.; Gruyaert, E. Increasing the reactivity of modified ferro silicate slag by chemical adaptation of the production process. In *Proceedings ICSBM 2019 Volume 4—Waste Recovery, Treatments and Valorization*; Caprai, V., Brouwers, J., Eds.; Technische Universiteit Eindhoven: Eindhoven, The Netherlands, 2019; pp. 36–46.
46. Lothenbach, B.; Le Saout, G.; Gallucci, E.; Scrivener, K. Influence of limestone on the hydration of Portland cements. *Cem. Concr. Res.* **2008**, *38*, 848–860. [[CrossRef](#)]
47. Kuzel, H.-J.; Pöllmann, H. Hydration of C3A in the presence of Ca(OH)₂, CaSO₄·2H₂O and CaCO₃. *Cem. Concr. Res.* **1991**, *21*, 885–895. [[CrossRef](#)]
48. Ipavec, A.; Gabrovšek, R.; Vuk, T.; Kaučič, V.; Maček, J.; Meden, A. Carboaluminate Phases Formation During the Hydration of Calcite-Containing Portland Cement. *J. Am. Ceram. Soc.* **2010**, *94*, 1238–1242. [[CrossRef](#)]
49. Kakali, G.; Tsivilis, S.G.; Aggeli, E.; Bati, M. Hydration products of C 3 A, C 3 S and Portland cement in the presence of CaCO₃. *Cem. Concr. Res.* **2000**, *30*, 1073–1077. [[CrossRef](#)]
50. Dweck, J.; Buchler, P.M.; Coelho, A.C.V.; Cartledge, F.K. Hydration of a Portland cement blended with calcium carbonate. *Thermochim. Acta* **2000**, *346*, 105–113. [[CrossRef](#)]
51. Péra, J.; Husson, S.; Guilhot, B. Influence of finely ground limestone on cement hydration. *Cem. Concr. Compos.* **1999**, *21*, 99–105. [[CrossRef](#)]
52. Krishnan, S.; Bishnoi, S. Understanding the hydration of dolomite in cementitious systems with reactive aluminosilicates such as calcined clay. *Cem. Concr. Res.* **2018**, *108*, 116–128. [[CrossRef](#)]
53. Matschei, T.; Lothenbach, B.; Glasser, F. The AFm phase in Portland cement. *Cem. Concr. Res.* **2007**, *37*, 118–130. [[CrossRef](#)]
54. Damidot, D.; Stronach, S.; Kindness, A.; Atkins, M.; Glasser, F. Thermodynamic investigation of the CaO–Al₂O₃–CaCO₃–H₂O closed system at 25 °C and the influence of Na₂O. *Cem. Concr. Res.* **1994**, *24*, 563–572. [[CrossRef](#)]
55. Min, D.; Mingshu, T. Formation and expansion of ettringite crystals. *Cem. Concr. Res.* **1994**, *24*, 119–126. [[CrossRef](#)]
56. Zajac, M.; Bremseth, S.K.; Whitehead, M.; Ben Haha, M. Effect of CaMg(CO₃)₂ on hydrate assemblages and mechanical properties of hydrated cement pastes at 40 °C and 60 °C. *Cem. Concr. Res.* **2014**, *65*, 21–29. [[CrossRef](#)]
57. Matschei, T.; Lothenbach, B.; Glasser, F. The role of calcium carbonate in cement hydration. *Cem. Concr. Res.* **2007**, *37*, 551–558. [[CrossRef](#)]